Applied Surface Science 601 (2022) 154230

Contents lists available at ScienceDirect

Applied Surface Science

journal homepage: www.elsevier.com/locate/apsusc

Full Length Article

Observation of robust superlubricity of MoS_2 on Au(111) in ultrahigh vacuum

Yiming Song [a], Antoine Hinaut [a], Sebastian Scherb [a], Yves Pellmont [a], Rémy Pawlak [a], Shuyu Huang [a,b], Zhao Liu [a], Thilo Glatzel [a,*], Ernst Meyer [a,*]

[a] Department of Physics, University of Basel, Klingelbergstrasse 82, 4056 Basel, Switzerland
[b] Key Laboratory for Design and Manufacture of Micro-Nano Biomedical Instruments, School of Mechanical Engineering, Southeast University, 211189 Nanjing, China

ARTICLE INFO

Keywords:
Superlubricity
Monolayer MoS_2
Moiré superlattice
Atomic force microscopy
Ultrahigh vacuum

ABSTRACT

The structural and superlubric properties of single layer MoS_2 on Au(1 1 1) forming moiré superlattice structures have been investigated by means of ultrahigh vacuum atomic force microscope with bimodal and contact modes. We synthesize epitaxial monolayer MoS_2 flakes on the Au(1 1 1) surface in ultrahigh vacuum. Using friction force microscopy, atomic friction measurements indicate a superlubric regime between the tip apex and the moiré corrugated MoS_2 surface in which the friction force remains at an ultralow value and is independent from normal load. Superlubricity conditions are observed for different loads and velocities which indicates the absence of out-of-plane deformations. We find that the MoS_2 layer including the moiré superlattice modulation originating from the natural misfit between MoS_2 and the Au(1 1 1) substrate is relatively rigid. We also demonstrate a low friction coefficient of the MoS_2 surface crossing a single Au(1 1 1) step. Our results open up a new avenue for minimizing friction in nanoscale electronic devices and other dry rigid contacts used in aerospace lubrication.

1. Introduction

Molybdenum disulfide (MoS_2), a single layer of Mo atoms sandwiched in between two layers of S atoms, shows a wide range of potential applications in the fields of electronics, optoelectronics and micro and nanomechanical systems requiring ultralow friction [1–2]. Due to its superior structural and mechanical characteristics, strong in-plane covalent bonding combined with weak interlayer van der Waals interaction, MoS_2 has been used as solid lubricant especially in aerospace applications [3]. At the nanoscale, extensive studies on frictional properties of MoS_2 revealed several intriguing characteristics, including normal load dependence [4–6], temperature/velocity dependence [6–10], contact size dependence [11–13], anisotropic directional dependence [14–15], orientational dependence [16–17], besides low friction and anti-wear performances [18]. In addition, another fascinating tribological phenomenon, in which friction decreases as the number of MoS_2 layers was increased, has also been revealed [19–20]. This layer dependence of friction was explained by the out-of-plane deformation in front of the sliding atomic force microscope (AFM) tip which is referred to as the puckering mechanism [19,21]. Meanwhile the out-of-plane deformation is also affected by the interfacial structure and adhesion between surface and substrate.

In previous research, the normal load dependence of friction between AFM tip and MoS_2 surface always shows a linear or logarithmic trend in different environments and conditions such as temperature, humidity and velocity [4–6]. However, all the previous preparation of MoS_2 film and corresponding nanoscale friction measurements were performed under ambient conditions. Therefore, the results can be significantly affected by contamination arising from adhesion layers on tip and sample (residue from transfer process, water or hydrocarbons). The constant change in surface conditions caused by the adsorption and desorption of atoms and molecules provides an additional channel for energy dissipation. Even if the measurements were done under ultrahigh vacuum (UHV) conditions, a typical positive load dependence of friction has been observed [6]. Contact quality between MoS_2 and substrate also plays another crucial role in frictional behavior, since out-of-plane deformation of the surface will increase the resistance during interfacial sliding. For this reason, single layer MoS_2 is always showing a higher energy dissipation and friction coefficient compared to multilayer structures [19–20]. Further studies show that friction of two-dimensional (2D) materials could be reduced significantly by the utilization of highly adhesive and atomic flat substrate to suppress the out-

* Corresponding authors.
E-mail addresses: thilo.glatzel@unibas.ch (T. Glatzel), Ernst.Meyer@unibas.ch (E. Meyer).

https://doi.org/10.1016/j.apsusc.2022.154230
Received 17 February 2022; Received in revised form 7 July 2022; Accepted 9 July 2022
Available online 12 July 2022

of-plane floppiness [19]. Therefore, the intrinsic frictional performance of MoS_2 is not clear since the friction dissipation is always covered by other dissipation mechanisms originating from aforementioned effects. To overcome this issue, a possible solution is to perform MoS_2 preparation and friction measurement under UHV conditions.

Here, we investigate the structural and frictional behaviors of MoS_2 superstructure on Au(1 1 1) and report the superlubricity between a bare Si AFM tip and MoS_2. The monolayer MoS_2 flakes of well controlled size are prepared under UHV conditions upon sputtering Mo atoms on an atomically clean Au(1 1 1) surface in H_2S atmosphere followed by post annealing. Both the moiré superstructure and the lattice structure of MoS_2 are detected with atomic resolution using bimodal UHV AFM. The investigation of the load dependence of the friction shows an independent correlation, in particular the absolute friction value is very low. Furthermore, we show the decrease of dissipative processes of monolayer MoS_2 when crossing a single step edge of the Au(1 1 1) surface. All measurements were performed at room temperature. Finally, the mechanism of superlubricity between the tip and MoS_2 is revealed using the Prandtl-Tomlinson (PT) model.

2. Results and discussions

Our main goal is to study the intrinsic frictional behavior between a sliding AFM tip and a well-defined MoS_2 surface with a moiré superlattice in a typical range of normal loads (maximum load is 8.5nN) and velocities (1.5 nm/s to 390 nm/s), and to identify conditions under which a superlubric state can be achieved. To this end, we prepare and analyze MoS_2 on Au(1 1 1) under UHV conditions. Mo is deposited on a freshly prepared Au(1 1 1) surface in an H_2S atmosphere (1.0×10^{-6} mbar) using an e-beam evaporator and then annealed at a temperature of 800 K, resulting in the growth of triangular MoS_2 flakes on the Au (1 1 1) substrate [22–24]. A topographic image of the surface of a typical epitaxial MoS_2 flake on the Au(1 1 1) substrate is shown in Fig. 1(a). The known moiré superlattice structure with 3.3 nm periodicity and height variation of ~ 45 pm was revealed by non-contact UHV AFM in the constant frequency shift mode at room temperature. This pattern is an indication of the lattice mismatch between the hexagonal lattice of MoS_2 and the single crystal Au(1 1 1) surface. In addition, the surface coverage could be tuned by increasing the amount of deposited Mo on the substrate [24–25]. The remaining bright spots shown in Fig. 1(a) represent deposited molybdenum which have not reacted with H_2S.

High resolution structural information of the MoS_2 surface is visible in a torsional AFM mode [26–28]. In this mode the frequency shift of the torsional oscillation Δf_{TR} is measured while controlling the tip sample distance either on the frequency shift of the first or second flexural oscillation in noncontact mode ensuring high resolution and stable scan conditions. A perfect MoS_2 atomic lattice and superstructure in high resolution are observed in Fig. 1(b), which demonstrates the high quality of the sample preparation. A lattice constant of 315 pm for the MoS_2 is determined, which is in good agreement with previous measurements [22]. The long-range moiré superlattice is also observed in the torsional mode having periodicity of 3.3 nm. Remarkably, we observed only one type of superstructure belonging to a particular alignment between the MoS_2 flakes and the Au(1 1 1) substrate, which was also shown in previous STM measurements [22–25]. We deduce that this alignment is due to a strong and specific bonding between MoS_2 and the Au(1 1 1) substrate resulting from a better commensurability and in good agreement with a recent experimental study [29].

Frictional force measurements are acquired in the same UHV AFM system using soft cantilevers in contact mode. These soft rectangular silicon cantilevers have normal and torsional spring constant of 0.28 N/m and 143.50 N/m, respectively. During the scanning in contact mode, the integral and the proportional gain of the feedback loop were set to low values, in order to avoid any influence of the feedback on the measurement of the lateral forces. Friction experiments were performed in areas of the sample in which both moiré corrugated MoS_2 and the bare Au(1 1 1) surface are present to be able to compare the tribological properties without the risk of major tip changes. The normal and lateral force acting on the tip were calibrated following the procedures given in Ref. [30].

Fig. 2(a) shows the frictional properties between the AFM tip and the MoS_2 on Au(1 1 1) (green), in which the averaged friction force is independent with increasing normal load at 12 nm/s scanning speed. In comparison, the same tip sliding on the bare Au(1 1 1) surface (blue) shows a strong positive dependence with a coefficient of friction (COF) of 0.28 ± 0.01 with the same velocity. It should be noted that we can quantitatively compare the friction force between surface with a moiré corrugated MoS_2 and Au(1 1 1) due to the *in-situ* measurements with the same tip and scanning velocities. The absolute value of friction force measured on the moiré corrugated MoS_2 surface is below 10 pN (averaged over all normal load configurations) which is more than two orders of magnitude smaller than the lowest value revealed on the Au(1 1 1) surface. Considering that the adhesion force on Au(1 1 1) is about 6 nN higher than that on MoS_2 (see supporting information for more details),

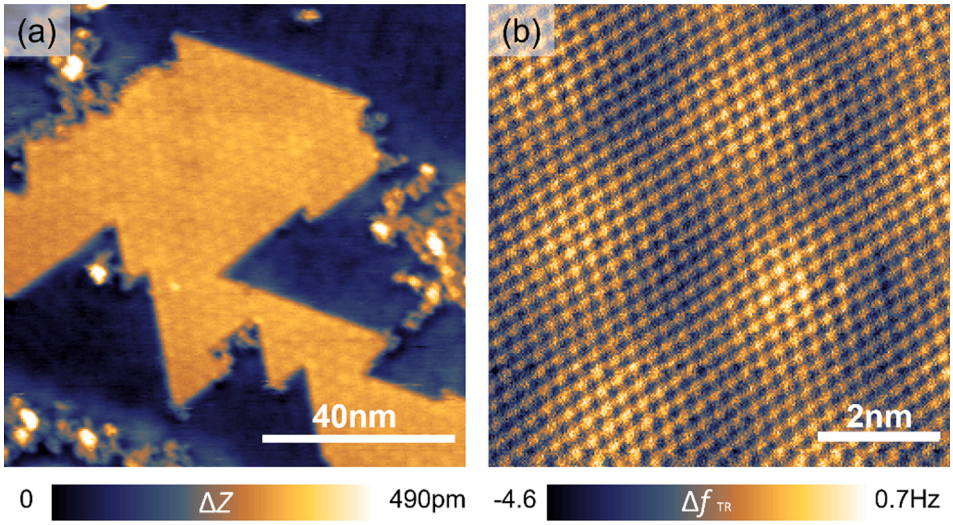

Fig. 1. Characterization of monolayer MoS_2 grown on Au(1 1 1) substrate in UHV. (a) 100 nm × 100 nm topographic nc-AFM image of a single layer MoS_2 flake. (b) High-resolution image showing the moiré and the atomic structure of the MoS_2 islands in the torsional frequency shift Δf_{TR} recorded in bimodal AFM. Parameters: (a) Δf_{1st} = -10 Hz, A_{1st} = 2.5 nm, (b) Δf_{2nd} = -100 Hz, A_{2nd} = 800 pm, A_{TR} = 80 pm.

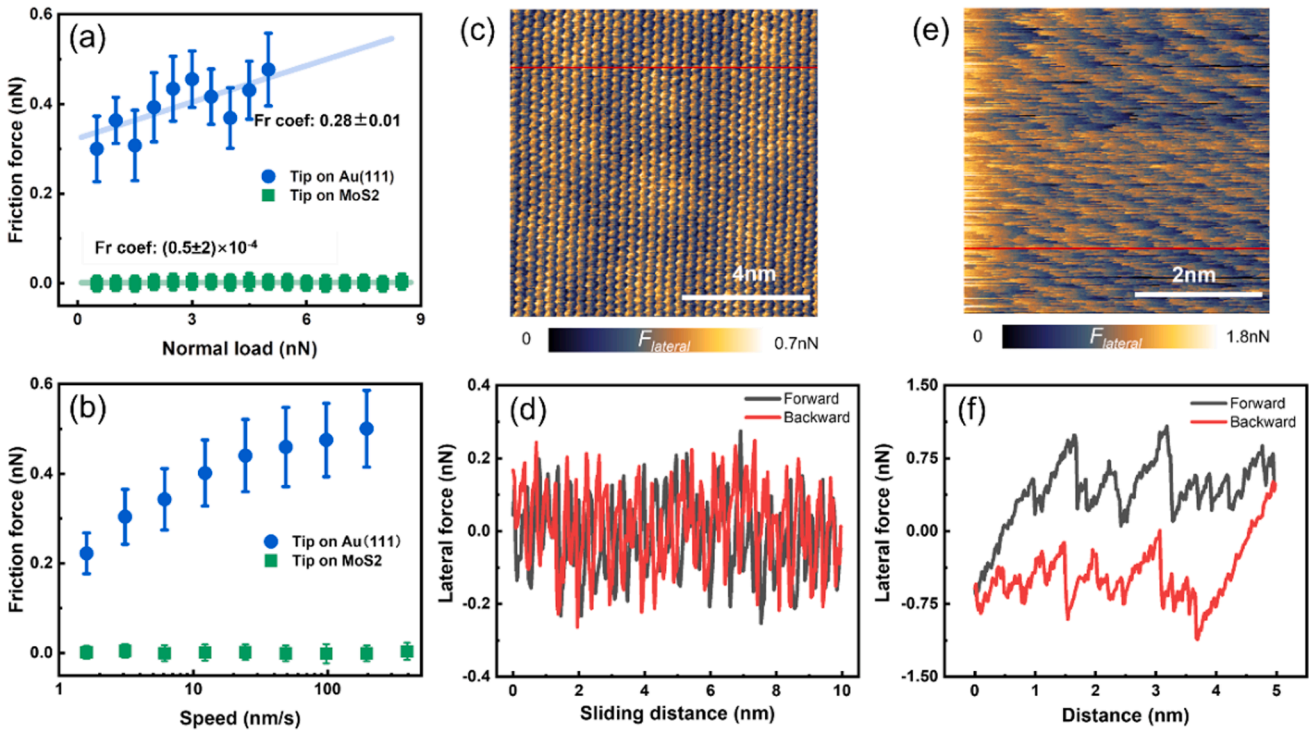

Fig. 2. Friction characterizations of MoS_2 and Au(1 1 1) surfaces. (a) Load dependence of the friction force between the Si AFM tip and the MoS_2 and Au(1 1 1) surfaces at a speed of 12 nm/s. (b) Dependence of the measured friction on the sliding velocity at a load of 5 nN (c, e) lateral force maps on the MoS_2 and Au(1 1 1) surfaces, respectively. (d, f) The lateral force loops in forward and backward direction indicated in the maps in (c, e), respectively, showing two different sliding behaviors of the scanning tip. The error bars represent the standard deviation of the repeated independent measurements.

which could contribute to a larger total normal load, yet this is not the critical factor that dominates such a strong frictional contrast in Fig. 2 (a). Thus, superlubric sliding exists between the AFM tip and the atomically clean MoS_2 surface with normal load independent frictional behavior up to 9 nN. The maximum load is limited by the spring constant of cantilever used in this work and the change of the tip or the substrate that should be avoided during the measuring process.

The lateral force reveals two opposite stick–slip profiles when scanning forward and backward on Au(1 1 1), as shown in Fig. 2(f). The area enclosed in this hysteresis loop is the energy dissipated in one sliding cycle. A completely different picture is found when the tip is sliding across the MoS_2 flake with moiré superstructure, as shown in Fig. 2(d). The hysteresis loop and with it the dissipation disappears within the sensitivity of the current measurement similar to the previous results [31]. Simultaneously, the sawtooth modulation of the lateral force is transformed into a continuous modulation of matching forward and backward scans, showing the atomic periodicity of the surface lattice. The scan velocity in both measurements was $v = 12$ nm/s.

The atomic scale structure and the moiré patterns in the lateral force map are also revealed in high resolution lateral force images (Fig. 2(c)). These results again confirm the cleanness, purity and high quality of the MoS_2 prepared and measured under UHV conditions. It guarantees the possibility to obtain the intrinsic frictional properties between tip apex and MoS_2 surface getting rid of other channels of energy dissipations, such as surface pollution and environmental conditions. Due to these advantages, we were able to demonstrate the superlubric regime between the bare tip apex and the MoS_2 surface, which bears no resemblance to the previous results [4–6]. Atomic defects were resolved in the lateral force map (see Fig. S4 in the supporting information), supporting the notion of a single-asperity tip sliding on the MoS_2 surface. For the measurements on the Au(1 1 1) substrate, the lateral force map (Fig. 2 (e)) also shows regular stick–slip motion comparable to previous results using silicon tips and metallic surfaces [32–33].

The velocity dependence of the friction measured on the two different surfaces is shown in Fig. 2(b), revealing, that the friction on Au (1 1 1) increases logarithmically with sliding speed which agrees well to the thermal activation method [34–36]. On the contrary, the friction on the moiré corrugated MoS_2 surface remains almost constant in the experimental range of speeds of 1.5 to 390 nm/s, in line with previous experimental observations [37]. All the measurements of frictional velocity dependence are conducted with 5 nN normal load. However, the exact origin of the constant friction force with increasing sliding velocity remains unclear.

To understand the origin of the experimentally measured frictional phenomena, a two-dimensional energy landscape was constructed and used as an input for the PT model [38–39]. The tip is dragged by a spring over a sinusoidal potential representing the interaction between the tip and the single-layer MoS_2 with amplitude E_0 and periodicity a. While sliding at constant velocity relative to the substrate a spring of effective spring constant K is tensioned between the tip apex position x_{tip} and the position of moving stage x_s. To include the long-range potential representing the moiré superstructure, an additional sinusoidal component is added to the short-range potential related to MoS_2 atomic structure as shown in Fig. 3(b). The rotation of the MoS_2 lattice by 0.45 degree with respect to the Au(1 1 1) structure is used in this model, which was also confirmed in our experiments (see the fast Fourier transform of the lateral force map in the supporting information in Fig. S5). The total potential experienced by the tip consists of three parts the tip-atom, the tip-moiré and the elastic interaction between the tip and the substrate. It writes as:

$$V(x,y) = V_{tip-atom} + V_{tip-moire} + V_{spring}, \tag{1}$$

where $V_{spring} = \frac{1}{2}K(x_{tip} - x_s)$, $V_{tip-MoS_2}$ and $V_{tip-moire}$ are 2D hexagonal potentials with the periodicity of MoS_2 lattice and the moiré structure. Both can be written in the same form.

$$V_{hexagonal}(\bar{x},\bar{y}) = E_0\left(2cos\frac{2\pi\bar{x}}{a}cos\frac{2\pi\bar{y}}{a\sqrt{3}} + cos\frac{4\pi\bar{y}}{a\sqrt{3}}\right). \tag{2}$$

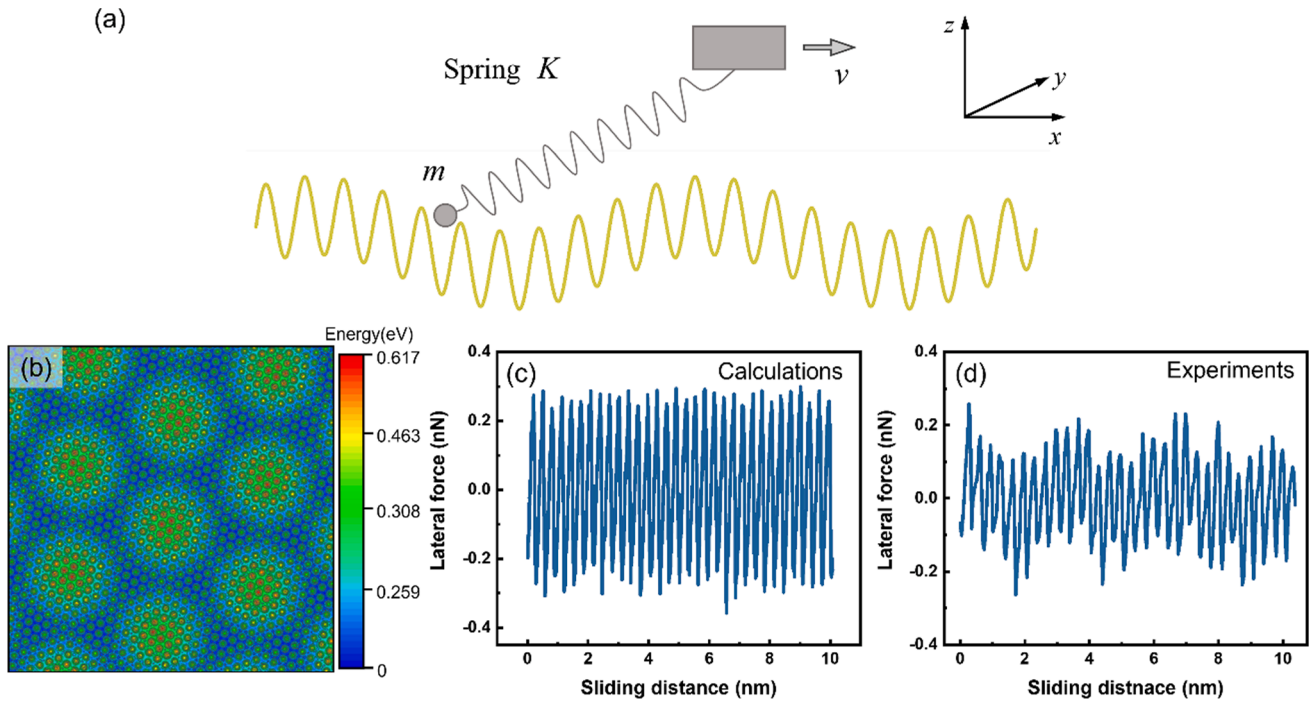

Fig. 3. Simulated superlubric sliding between a point mass and a hexagonal lattice with super structure. (a) Schematics of the PT model. The tip is dragged over a moiré tuning double-periodic potential corrugation moving at a constant velocity, v. (b) Energy landscape exhibiting two periodicities due to the superlattice structure corresponding to MoS_2 on Au(1 1 1). (c) Lateral force predicted *via* PT model simulation with $l_{\_MoS2} = 0.315$ nm, $l_{\_Au(1\,1\,1)} = 0.288$ nm, relative rotation angel $\theta = 0.45$ degrees, $E_{0\_MoS2} = 0.08$ eV, $E_{0\_moiré} = 0.056$ eV, $m = 10^{-12}$ kg, $v = 15$ nm/s, $K = 6.35$ N/m, damping coefficient $\gamma = 2\sqrt{K/m}$, $T = 300$ K. (d) experimental measurements with the same sliding speed 15 nm/s and temperature $T = 300$ K as used in (c) and normal load at 3.5 nN.

The amplitude of the potential corrugation of the MoS_2 surface E_{0_MoS2} can be calculated by $E_0 = \frac{aF_L^{max}}{\pi}$ according to the Ref. [31]. Thus, the amplitude of energy corrugation of MoS_2 is 0.08 eV, which is determined directly from experimental measurements and shows a quite flat energy profile, consistent with the ultra-low friction observed in the experiments.

The two different sliding movements depend on the relation between E_0 and the elastic energy which can be described by the dimensionless parameter $\eta = \frac{4\pi^2 E_0}{Ka^2}$. We can also determine η as $\eta = \frac{2\pi F_L^{max}}{k_{exp} a} - 1$ by a detailed analysis of the experimental results [40]. In our case, η is 0.44 lower than 1 with a vanishing stick–slip process which means a superlubric state has been achieved between the AFM tip and the MoS_2 surface. Smooth sliding motion results in the vanishing of energy dissipation. Then the effective spring constant can be calculated with the formula $K = \frac{\eta+1}{\eta} k_{exp}$. Now only one parameter, the amplitude of the potential of the moiré superlattice $E_{0\_moiré}$ is not determined. It is expected that the ratio β between the amplitudes of the superstructure potential $E_{0\_moiré}$ and the atomic potential E_{0_MoS2} is lower than 1 [38]. A satisfying agreement between simulation and experimental results was obtained by using $\beta = 0.7$. Furthermore, the value of β corresponds to the one used in Ref. [38] for a similar system. Thus, we could model the 2D potential corrugation of single layer MoS_2 on Au(1 1 1) substrate as shown in Fig. 3(b). Except for β, all the parameters used in the PT model simulations are chosen based on the experimental parameters, which leads to an excellent agreement that the simulation well reproduces the friction measurements as shown in Fig. 3(c). The absolute value and moiré profile of the lateral force can be compared directly to the experimental results (Fig. 3(d)) due to the used realistic parameters also quantitatively. Furthermore, not only the periodicities of the lattice spacing but the moiré modulation of lateral force in both experiments and simulations are in good agreements, which indicates that MoS_2 including the superstructure is relatively rigid and can be accurately described by the PT model, where deformations are neglected. The rigidity of moiré corrugated MoS_2 surface is due to the strong in-plane covalent bonding combined with strong interaction between monolayer MoS_2 and Au(1 1 1) surface.

The existence of the superlubric state between AFM tip and MoS_2 is influenced by two opposite effects related to the strong interaction of monolayer MoS_2 and Au(1 1 1) and the additional potential created by the long-range superlattice structure. Au is known to have a strong affinity for sulfur, therefore the strong interaction between gold and the MoS_2 surface tightly anchor the single layer onto the substrate [22,37]. Recent experimental and theoretical studies [29] have also confirmed that hybridization between S orbitals and states of the gold substrate is the main contribution to strong binding. This leads to the suppression of local out-of-plane deformation when the layer is scanned with the AFM tip. Experimentally, this is confirmed by the disappearance of the so called “strengthening” effect [19] as apparent in Fig. 2(d), which shows no gradual transient of the static friction force. This effect is based on the change in the quantity and quality of atomic scale contacts below the tip during the sliding process [21]. On the other hand, the nearly aligned configuration between Au(1 1 1) and the MoS_2 layer not only reduces friction, but also forms a superstructure that provides an additional corrugated potential, leading to a corresponding change in friction. In the case of a KBr layer on Cu(1 1 1), the energy dissipation is caused by a superlattice structure due to a tiny rumpling in the vertical direction [41]. In contrast, no variation in the energy dissipation of graphene on SiC(0001) with modulated moiré structure is observed, as the trace and retrace of friction are consistently changed [39,42] In our measurements, the height corrugation of the moiré superlattice is about 45 pm with a periodicity of 3.3 nm, indicating that the friction force modulated by moiré pattern is much smaller than that induced by the atomic structure. The lateral force trace and retrace coincide very well, also leading to the result that there is almost no variation of the energy dissipation due to the smaller amplitude of the potential and the larger periodicity of the long-range superstructure [34]. The moiré corrugation is no more than 0.1 nm, which is confirmed in our measurement also in

agreement with the recent low temperature STM measurements [29]. These two competing effects are the dominant ones in sliding under the premise of measuring the intrinsic friction force between the tip apex and the atomically clean moiré corrugated MoS_2 surface. Otherwise, impurities or water adsorption would provide additional energy dissipation channels, which would dominate the energy dissipation process leading to the elimination of superlubricity, as shown in previous results [4–6]. In conclusion, the superlubric sliding between the tip apex and the MoS_2 moiré superlattice can be achieved due to the reconstruction and a well-defined sliding interface.

An important factor that needs to be taken into account for practical application of single layer MoS_2 as solid lubricant is the effect of step edges of the substrate, specifically, the influence of topographical effects on the measured friction [43–45]. The full suppression of step edges of metal surfaces is impossible. Based on the present synthesis, a nearly perfect hexagonal MoS_2 flake which is overlaid on an Au(1 1 1) step edge is illustrated in Fig. 4(a). The inset of Fig. 4(a) shows the height profile parallel to the fast scanning direction and shows the height of a single atomic step of Au(1 1 1) which is ~ 0.26 nm consistent with Ref. [46]. The tip moving upward along the MoS_2 layer crossing a single Au(1 1 1) step experiences extra resistance compared to the tip moving on the flat surface which originated from the topographical effect. Similarly, the tip moving downward faces less resistance [47].

A typical lateral force slide during the trace and retrace moving on the MoS_2 surface and crossing an Au step is shown in Fig. 4(b). Since the forward and backward scan almost match with each other within the experimental error, there is no chemical interaction between the tip apex and the MoS_2 surface [45]. To evaluate the topographical effect on the friction, we investigated the maximum lateral force F_m during tip sliding across the buried step edge covered with a single layer MoS_2. The rate of change of F_m with normal load along upward and downward scanning is used to quantify the COF. Compared to the 10^{-5} COF obtained from the basal plane measurements within the superlubric regime, the COFs during both upward and downward increase by 4 orders of magnitude (Fig. 4(c)). Both upward and downward scan directions show the same dependence on the applied normal load. We note that the COF calculated from F_m is still lower than the value from the Au (1 1 1) substrate. More importantly, only the absolute maximum lateral force is quite high and increases with the normal load, the total dissipation through the whole scanning line keeps at a very low level even in the area of the buried step.

Finally, another key factor for realistic tribological scenarios is the ability to remain in low friction at different sliding velocities. To this end, we measured the dependence of F_m on the sliding velocity up to 390 nm/s. As demonstrated in Fig. 4(d), the maximum lateral force increases only slowly with the sliding velocities. However, as already mentioned before in the regime of superlubric states, the velocity dependence of a contact crossing buried step edge is still not very well understood and needs further attention as well.

In summary, we characterized the structural and frictional properties of epitaxial single layer MoS_2 grown on a monocrystalline Au(1 1 1) surface under UHV. The surface lattice of MoS_2 was resolved with atomic resolution using bimodal UHV AFM at room temperature, unveiling the moiré superlattice (3.3 nm periodicity) and the MoS_2 atomic structure. We also demonstrated the experimental capability to achieve a robust superlubric state between a sliding Si tip and moiré corrugated MoS_2 surface, which shows an ultralow friction behavior independent to the normal load. MoS_2 moiré superlattice coverage ensures good tribological performance even in areas crossing Au(1 1 1) step edges. Our calculations demonstrate excellent agreement with the experimental data. This indicates that superlubricity is intimately connected to the relatively rigid structure of the MoS_2 layer including the superstructure induced by lattice mismatch between MoS_2 and the Au (1 1 1) substrate. Consequently, the out-of-plane deformations are suppressed strongly, and the additional friction induced by extra potential originating from the superlattice can be neglected. Such results reveal atomistic insight into fundamental mechanism of ultralow friction and are expected to be applicable for other sliding contact interfaces.

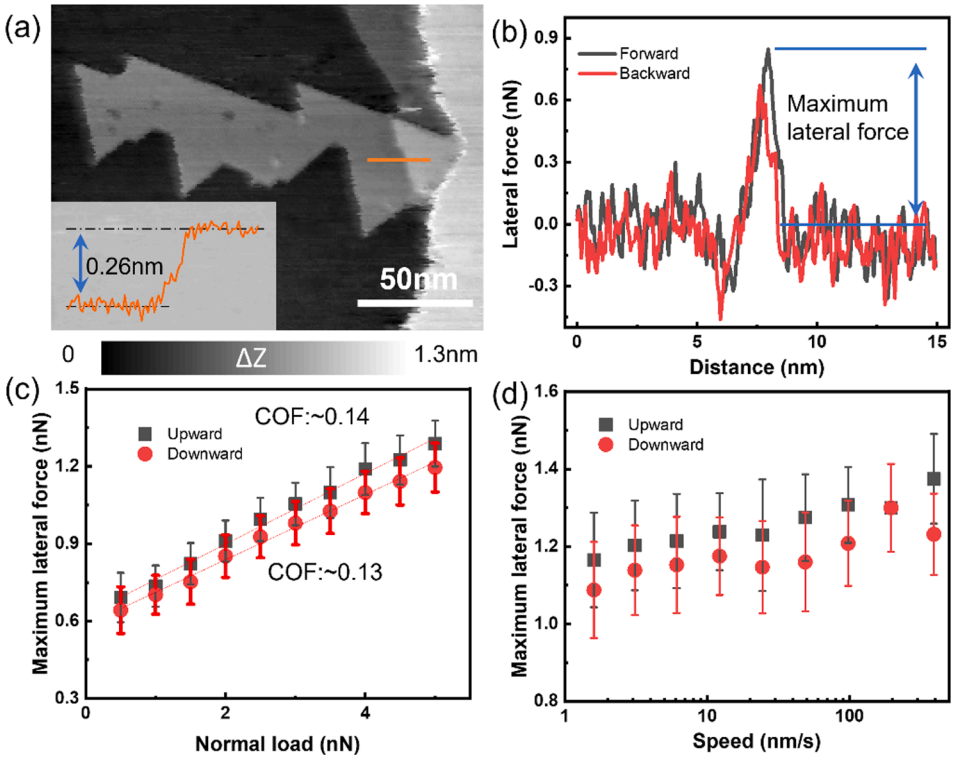

Fig. 4. Topography and frictional forces of MoS_2 islands crossing single Au(1 1 1) step edges. (a) Topography in a large scan area measured in contact mode. The inset shows a height profile along a buried Au(1 1 1) step edge covered with a monolayer MoS_2. (b) Typical lateral force loop across a buried step edge. (c, d) Load and velocity dependence of the maximum lateral force between AFM tip and MoS_2 surface crossing a single Au(1 1 1) step. The error bars represent the standard deviation of the repeated independent measurements.

3. Methods

3.1. Sample preparation

Single-layer MoS_2 flakes were grown in a UHV chamber (base pressure of $< 5 \times 10^{-10}$ mbar) on a freshly prepared Au(1 1 1) single-crystal surface. The Au(1 1 1) surface was prepared by several cycles of Ar^+ ion sputtering (~2000 eV, 3×10^{-6} mbar Ar pressure and 10–15 min) and annealing (750 K, 10–20 min). The cleanliness of the surface was verified by the presence of the Au herringbone reconstruction by nc-AFM (see Fig. S1 in the supporting information). MoS_2 was prepared according to Ref. [26–27]. by molybdenum deposition and H_2S dosing. Molybdenum was deposited onto the Au(1 1 1) surface *via* electron beam evaporating for 5 min while the H_2S gas was dosed directly to the sample through a nozzle at a distance of 5–10 mm. Pressure of the preparation chamber keeps at 10^{-6} mbar during the process. Afterwards, the sample was annealed at 800 K for half an hour. Then, the sample was transferred to the UHV AFM system *via* an UHV transfer suitcase (base pressure of $< 5 \times 10^{-10}$ mbar).

3.2. AFM measurements

Non-contact and friction force AFM measurements were performed with a home-built microscope using beam deflection detection with a bandwidth of 3 MHz. Topography of MoS_2 was obtained by using the first flexural mode of the cantilever (PPP-NCL, nanosensors) with a center frequency of $f_{1st} = 172$ kHz and an amplitude of $A_{1st} = 2.5$ nm. The typical quality factor of these cantilevers in UHV is $Q_{1st} = 30\,000$. Bimodal experiments were also conducted by using the first phase locked loop (PLL) to control the tip-sample distance and a second PLL to drive the first torsional oscillation mode with values typically around $f_{TR} = 1.7$ MHz, an amplitude of $A_{TR} = 80$ pm, and quality factor of $Q_{TR} = 60\,000$. Friction force measurements were performed in contact mode with a silicon cantilever (PPP-CONTR, nanosensors) at specific speeds and normal loads. A very slow feedback loop on the normal load controlling the tip-sample distance was used, in order to avoid any influence of the feedback on the measurement of the lateral forces.

CRediT authorship contribution statement

Yiming Song: Investigation, Methodology, Formal analysis, Writing – original draft. **Antoine Hinaut:** Methodology, Investigation, Writing – review & editing. **Sebastian Scherb:** Investigation, Writing – review & editing. **Yves Pellmont:** Resources, Writing – review & editing. **Rémy Pawlak:** Writing – review & editing. **Shuyu Huang:** Investigation, Writing – review & editing. **Zhao Liu:** Writing – review & editing. **Thilo Glatzel:** Conceptualization, Methodology, Formal analysis, Writing – review & editing. **Ernst Meyer:** Conceptualization, Supervision, Formal analysis, Writing – review & editing, Funding acquisition.

Declaration of Competing Interest

The authors declare that they have no known competing financial interests or personal relationships that could have appeared to influence the work reported in this paper.

Data availability

Data will be made available on request.

Acknowledgement

We would like to thank Christian Lotze from the Free University of Berlin for the discussions and support in installing the special MoS2 preparation chamber. The authors also gratefully thank the Nano Imaging Lab especially Miss Evi Bieler for the support of SEM characterization of the cantilever. Financial support from the Swiss National Science Foundation (SNSF) and the Swiss Nanoscience Institute (SNI) is gratefully acknowledged. We also thank the European Research Council (ERC) under the European Union's Horizon 2020 research and innovation program (ULTRA-DISS Grant Agreement No. 834402) and the European Commission under the FET-Open program (Q-AFM Grant Agreement No. 828966).

Appendix A. Supplementary material

Supplementary data to this article can be found online at https://doi.org/10.1016/j.apsusc.2022.154230.

References

[1] A.K. Geim, I.V. Van der Grigorieva, Waals heterostructures, Nature 499 (7459) (2013) 419–425.
[2] O. Hod, E. Meyer, Q. Zheng, M. Urbakh, Structural superlubricity and ultralow friction across the length scales, Nature 563 (7732) (2018) 485–492.
[3] E.W. Roberts, Space tribology: its role in spacecraft mechanisms, J. Phys. D-Appl. Phys. 45 (50) (2012) 503001.
[4] M.R. Vazirisereshk, H. Ye, Z. Ye, A. Otero-de-la-Roza, M.-Q. Zhao, Z. Gao, A.T. C. Johnson, E.R. Johnson, R.W. Carpick, A. Martini, Origin of Nanoscale Friction Contrast between Supported Graphene, MoS2, and a Graphene/MoS2 Heterostructure, NANO Lett 19 (8) (2019) 5496–5505.
[5] B.C. Tran-Khac, H.J. Kim, F.W. DelRio, K.H. Chung, Operational and environmental conditions regulate the frictional behavior of two-dimensional materials, Appl. Surf. Sci. 483 (2019) 34–44.
[6] X.Y. Zhao, S.R. Phillpot, W.G. Sawyer, S.B. Sinnott, S.S. Perry, Transition from thermal to athermal friction under cryogenic conditions, Phys. Rev. Lett. 102 (2009) (18).
[7] O. Acikgoz, M.Z. Baykara, Speed dependence of friction on single-layer and bulk MoS2 measured by atomic force microscopy, Appl. Phys. Lett. 116 (7) (2020) 071603.
[8] H.S. Khare, D.L. Burris, The effects of environmental water and oxygen on the temperature-dependent friction of sputtered molybdenum disulfide, Tribol. Lett. 52 (3) (2013) 485–493.
[9] P.E. Sheehan, C.M. Lieber, Friction between van der Waals solids during lattice directed sliding, NANO Lett. 17 (7) (2017) 4116–4121.
[10] J.F. Curry, A.R. Hinkle, T.F. Babuska, M.A. Wilson, M.T. Dugger, B.A. Krick, N. Argibay, M. Chandross, Atomistic origins of temperature-dependent shear strength in 2D materials, Acs Appl. Nano Mater. 1 (10) (2018) 5401–5407.
[11] D. Dietzel, J. Brndiar, I. Stich, A. Schirmeisen, Limitations of structural superlubricity: chemical bonds versus contact size, ACS Nano 11 (8) (2017) 7642–7647.
[12] H. Li, J. Wang, S. Gao, Q. Chen, L. Peng, K. Liu, X. Wei, Superlubricity between MoS2 monolayers, Adv. Mater. 29 (27) (2017) 1701474.
[13] X. Zhou, Y. Liu, X. Hu, L. Fang, Y. Song, D. Liu, J. Luo, Influence of elastic property on the friction between atomic force microscope tips and 2D materials, Nanotechnology 31 (28) (2020) 285710.
[14] M.R. Vazirisereshk, K. Hasz, R.W. Carpick, A. Martini, Friction anisotropy of MoS2: effect of tip-sample contact quality, J. Phys. Chem. Lett. 11 (16) (2020) 6900–6906.
[15] P.E. Sheehan, C.M. Lieber, Nanotribology and nanofabrication of MoO3 structures by atomic force microscopy, Science 272 (5265) (1996) 1158–1161.
[16] M. Liao, P. Nicolini, L. Du, J. Yuan, S. Wang, H. Yu, J. Tang, P. Cheng, K. Watanabe, T. Taniguchi, L. Gu, V.E.P. Claerbout, A. Silva, D. Kramer, T. Polcar, R. Yang, D. Shi, G. Zhang, UItra-low friction and edge-pinning effect in large-lattice-mismatch van der Waals heterostructures, Nat. Mater. 21 (1) (2022) 47–53.
[17] J.M. Martin, C. Donnet, T. Le Mogne, T. Epicier, Superlubricity of molybdenum disulphide, Phys. Rev. B Condens. Matter. 48 (14) (1993) 10583–10586.
[18] Y. Liu, A. Song, Z. Xu, R. Zong, J. Zhang, W. Yang, R. Wang, Y. Hu, J. Luo, T. Ma, Interlayer friction and superlubricity in single-crystalline contact enabled by two-dimensional flake-wrapped atomic force microscope tips, ACS Nano 12 (8) (2018) 7638–7646.
[19] C. Lee, Q. Li, W. Kalb, X.Z. Liu, H. Berger, R.W. Carpick, J. Hone, Frictional characteristics of atomically thin sheets, Science 328 (5974) (2010) 76–80.
[20] L. Fang, D.-M. Liu, Y. Guo, Z.-M. Liao, J.-B. Luo, S.-Z. Wen, Thickness dependent friction on few-layer MoS2, WS2, and WSe2, Nanotechnology 28 (24) (2017) 245703.
[21] S. Li, Q. Li, R.W. Carpick, P. Gumbsch, X.Z. Liu, X. Ding, J. Sun, J. Li, The evolving quality of frictional contact with graphene, Nature 539 (7630) (2016) 541–545.
[22] S.G. Sorensen, H.G. Fuchtbauer, A.K. Tuxen, A.S. Walton, J.V. Lauritsen, Structure and electronic properties of in situ synthesized single-layer MoS2 on a gold surface, ACS Nano 8 (7) (2014) 6788–6796.
[23] N. Krane, C. Lotze, J.M. Lager, G. Reecht, K.J. Franke, Electronic structure and luminescence of quasi-freestanding MoS2 nanopatches on Au(111), NANO Lett 16 (8) (2016) 5163–5168.
[24] N. Krane, C. Lotze, K.J. Franke, Moire structure of MoS2 on Au(111): Local structural and electronic properties, Surf. Sci. 678 (2018) 136–142.
[25] S.S. Gronborg, S. Ulstrup, M. Bianchi, M. Dendzik, C.E. Sanders, J.V. Lauritsen, P. Hofmann, J.A. Miwa, Synthesis of epitaxial single-layer MoS2 on Au(111), Langmuir: ACS J. Surf. Colloids 31 (35) (2015) 9700–9706.

[26] S. Kawai, T. Glatzel, S. Koch, B. Such, A. Baratoff, E. Meyer, Systematic achievement of improved atomic-scale contrast via bimodal dynamic force microscopy, Phys. Rev. Lett. 103 (2009) (22).
[27] N.F. Martinez, S. Patil, J.R. Lozano, R. Garcia, Enhanced compositional sensitivity in atomic force microscopy by the excitation of the first two flexural modes, Appl. Phys. Lett. 89 (15) (2006).
[28] J.R. Lozano, R. Garcia, Theory of multifrequency atomic force microscopy, Phys. Rev. Lett. 100 (7) (2008).
[29] C.C. Silva, D. Dombrowski, N. Atodiresei, W. Jolie, F.F. zum Hagen, J.Q. Cai, P.T.P. Ryan, P.K. Thakur, V. Caciuc, S. Blugel, D.A. Duncan, T. Michely, T.L. Lee, C. Busse, Spatial variation of geometry, binding, and electronic properties in the moire superstructure of MoS2 on Au(111), 2d Materials 9 (2) (2022).
[30] E. Meyer, H.J. Hug, R. Bennewitz, Scanning Probe Microscopy: The Lab on a Tip, first ed., Springer-Verlag, Berlin Heidelberg, 2004.
[31] A. Socoliuc, R. Bennewitz, E. Gnecco, E. Meyer, Transition from stick-slip to continuous sliding in atomic friction: entering a new regime of ultralow friction, Phys Rev Lett 92, (13) (2004), 134301.
[32] R. Bennewitz, E. Gnecco, T. Gyalog, E. Meyer, Atomic friction studies on well-defined surfaces, Tribol. Lett. 10 (1–2) (2001) 51–56.
[33] R. Bennewitz, T. Gyalog, M. Guggisberg, M. Bammerlin, E. Meyer, H.J. Guntherodt, Atomic-scale stick-slip processes on Cu(111), Phys. Rev. B 60 (16) (1999) R11301–R11304.
[34] A. Vanossi, N. Manini, M. Urbakh, S. Zapperi, E. Tosatti, Colloquium: modeling friction: From nanoscale to mesoscale, Rev. Mod. Phys. 85 (2) (2013) 529–552.
[35] E. Gnecco, R. Bennewitz, T. Gyalog, C. Loppacher, M. Bammerlin, E. Meyer, H. Guntherodt, Velocity dependence of atomic friction, Phys. Rev. Lett. 84 (6) (2000) 1172–1175.
[36] E. Riedo, E. Gnecco, R. Bennewitz, E. Meyer, H. Brune, Interaction potential and hopping dynamics governing sliding friction, Phys. Rev. Lett. 91, (8) (2003), 084502.
[37] X. Zheng, L. Gao, Q. Yao, Q. Li, M. Zhang, X. Xie, S. Qiao, G. Wang, T. Ma, Z. Di, J. Luo, X. Wang, Robust ultra-low-friction state of graphene via moire superlattice confinement, Nat. Commun. 7 (2016) 13204.
[38] P. Steiner, E. Gnecco, T. Filleter, N.N. Gosvami, S. Maier, E. Meyer, R. Bennewitz, Atomic friction investigations on ordered superstructures, Tribol. Lett. 39 (3) (2010) 321–327.
[39] T. Filleter, R. Bennewitz, Structural and frictional properties of graphene films on SiC(0001) studied by atomic force microscopy, Phys. Rev. B 81 (2010) (15).
[40] E. Gnecco, R. Bennewitz, T. Gyalog, E. Meyer, Friction experiments on the nanometre scale, J. Phys.-Condens. Mat. 13 (31) (2001) R619–R642.
[41] S. Maier, E. Gnecco, A. Baratoff, R. Bennewitz, E. Meyer, Atomic-scale friction modulated by a buried interface: combined atomic and friction force microscopy experiments, Phys. Rev. B 78 (4) (2008) 5.
[42] Y. Dong, A. Vadakkepatt, A. Martini, Analytical models for atomic friction, Tribol. Lett. 44 (3) (2011) 367–386.
[43] H. Holscher, D. Ebeling, U.D. Schwarz, Friction at atomic-scale surface steps: experiment and theory, Phys. Rev. Lett. 101 (24) (2008).
[44] Z. Chen, A. Khajeh, A. Martini, S.H. Kim, Chemical and physical origins of friction on surfaces with atomic steps, Sci. Adv. 5 (8) (2019).
[45] Z. Chen, A. Khajeh, A. Martini, S.H. Kim, Identifying physical and chemical contributions to friction: a comparative study of chemically inert and active graphene step edges, Acs Appl. Mater. Inter. 12 (26) (2020) 30007–30015.
[46] R. McHardy, W.H. Haiss, R.J. Nichols, An STM investigation of surface diffusion on iodine modified Au(111), PCCP 2 (7) (2000) 1439–1444.
[47] H. Lee, H.B.R. Lee, S. Kwon, M. Salmeron, J.Y. Park, Internal and external atomic steps in graphite exhibit dramatically different physical and chemical properties, ACS Nano 9 (4) (2015) 3814–3819.